TICRA

In-flight Retrieval of Geometrical information on the Planck Telescope

RF performance of detectors extended with wide-band nature for second retrieved geometry,

RFM2

Author: Per Heighwood Nielsen

April, 2016 S-1599-WP4

TICRA
LÆDERSTRÆDE 34 · DK-1201 COPENHAGEN K DENMARK
TELEPHONE +45 33 12 45 72 TELEFAX +45 33 12 08 80
E-MAIL ticra@ticra.com http://www.ticra.com

VAT REGISTRATION NO. DK-1055 8697
TICRA FOND, CVR REG. NO. 1055 8697

TABLE OF CONTENTS

1. Introduction.

The present study is prepared for ESTEC under contract no. 18395/04/NL/NB, CCN no. 9.

The title of the work is

"RF performance of all detectors for first retrieved geometry, RFM1"

The work was previously performed and reported in S-1599-WP1. This project is a follow-up for the second retrieved geometry, RFM2, and is initiated to calculate all the main beams for one selected detector in each frequency band from 30 GHz and up to 353 GHZ. The calculations are performed for one selected polarization only, but for all possible frequencies in the frequency bands. Furthermore, the average power patterns are calculated incorporating the effect of the amplifier losses of the detectors at the different frequencies in the frequency bands. The knowledge available on the RF performance of Planck is built mainly from three sources:

1. The second retrieved Planck telescope geometry, RFM2, described in TICRA report S-1563-13 but without any satellite shield structures, see Appendix A.

2. Spherical wave expansions of the detectors at different frequencies in the frequency bands.

3. The amplifier losses of the detectors as function of the frequencies in the frequency bands

The detectors are selected in Chapter 2.

All the calculated RF patterns are delivered to ESTEC in GRASP formatted grid files, in Co and Cx components and in the Pxx coordinate system described in Chapter 3.

The wide-band nature of the LFI main beams for the three detectors in the calculations is examined in Chapter 4 and the four HFI beams are investigated in Chapter 5. For all detectors the bandpass main beam is calculated and the differences from the used single frequency beams in the previous retrievals are evaluated.

2. Selected Detectors.

The detectors in the different frequency bands are selected for the following reasons.

LFI detectors

30 GHz: LFI27S, this detector is used in the 4pi calculations in Report S-1599-02

44 GHz: LFI25S, the retrieved variance is 0.13 dB in report S-1563-14 Table 3-1, which is the average of all the 44 GHZ beams.

70 GHz: LFI19S, the retrieved variance is 0.10 dB in report S-1563-14 Table 3-1, which is the average of all the 70 GHZ beams.

HFI detectors

100 GHz: HFI_100_3a, the false measured ripples on the 20 dB contour curves are small, see Figure 2-5 in report S-1563-15.

143 GHz: HFI_143_2a, the false measured ripples on the 20 dB contour curves are small, see Figure 2-11 and Figure 2-18 in report S-1563-15.

217 GHz: HFI_217_6a, the false measured ripples on the 20 dB contour curves are small, see Figure 2-26 in report S-1563-15.

353 GHz: HFI_353_5b, having the largest difference, see Table 3-1 in Report S-1563-15, but the smallest measured ripples.

For the 30 GHz detectors 7 RF horn patterns at different frequencies inside the bandwidth have been calculated and delivered by ESTEC together with 5 RF horn patterns for all the other detectors. The detector patterns were previously expanded to spherical modes and used in the RFFM calculation in report S-1496-3a.

3. RF performance.

All simulated main beam patterns will be analysed using Physical Optics on both mirrors and calculated in uv directions defined in the P_{xx} coordinate system for each beam as

$$u = \sin(\theta)\cos(\varphi)$$
$$v = \sin(\theta)\sin(\varphi)$$

The P_{xx} coordinate system is defined in the Planck Parameter Definition Document. Here the z-axis is pointing towards the main beam maximum and the x-axis is aligned with the polarization main axis. These values are found from the calculated main beams at the centre frequency using the pattern_characteristic object in GRASP. In the following sections the P_{xx} coordinate systems are presented by the unit vectors of the x-, y- and z-axis in the Field-Of-View, FOV, coordinate system or in the GRASP angles as defined in the GRASP Technical Description.

The patterns are limited to 2.5x2.5 degrees (u,v=0.044,0.044) for the LFI detectors and 80x80 arcmin (u,v=0.024,0.024) for the HFI detectors. The previous RFFM fields in report S-1496-3a were calculated with the grid limit listed in Table 3-1. In order to have the same increments giving around 14 directions over the HPBW, the new field grids must have the sizes shown. At 353 GHz the grid size is then 801*801 and the file size around 46 Mb.

fields grid	old 101*101		new grid size	
frequency	limits	Increment	±2.5 degrees	±80 arcmin
30 GHZ	0.0330	0.000660	135	
44 GHz	0.0230	0.000460	193	
70 GHz	0.0150	0.000300	295	
100 GHz	0.0100	0.000200		241
143 GHz	0.0070	0.000140		345
217 GHz	0.0046	0.000092		523
353 GHz	0.0030	0.000060		801

Table 3-1 Field grids.

The number of calculated field patterns is 37 (17 LFI and 20 HFI). The patterns are delivered as Co and Cx components in GRASP formatted uv-grid files. The syntax of the files is the same as in Report S-1496-3a. E.g. the field for HFI detector 100_1 at centre frequency, f3, and in x-polarization has the file name hfi_100_1_f3_x.grd.

The effect of the amplifier losses of the detectors at different frequencies in the frequency bands is calculated giving the average power beams for all the selected wide-band detectors. The differences from the used single frequency beams are evaluated.

4. LFI bandpasses.

In this Chapter the LFI bandpasses delivered from ESTEC are used to simulate the influence on the main beams measured. All the radiometer bandshapes are shown in Figure 4-1.

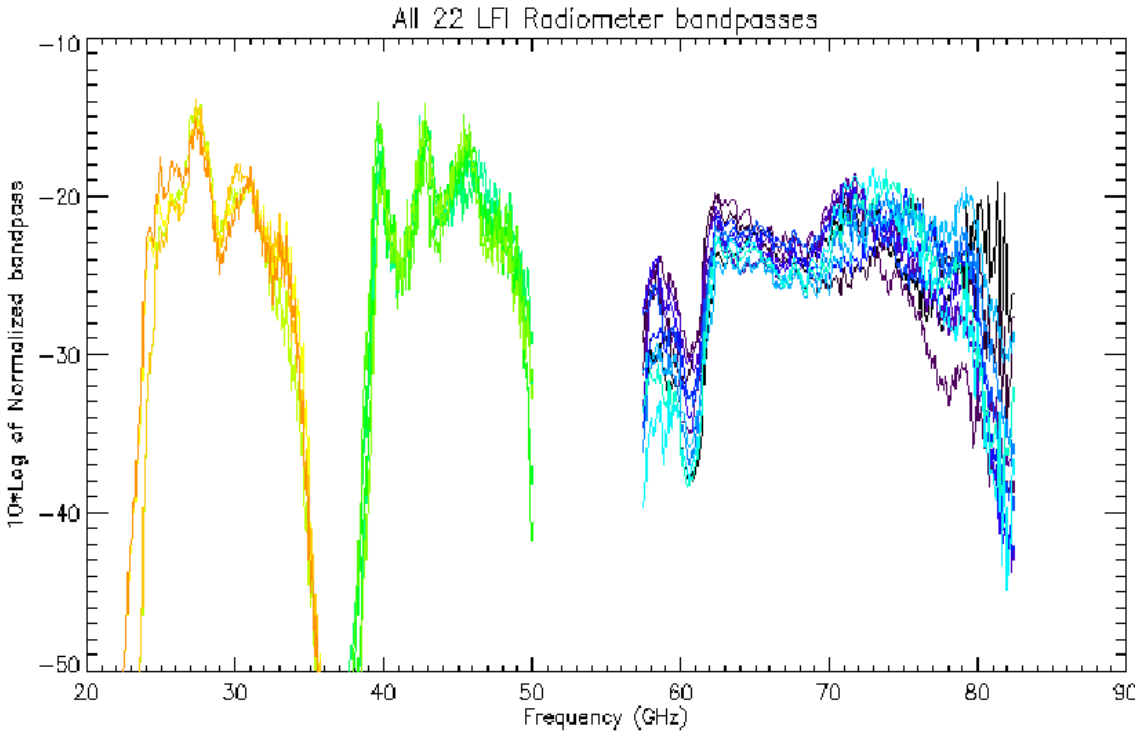

Figure 4-1 All LFI bandpasses.

The radiometer bandshapes in Figure 4-1 have to be averaged in different frequency intervals depending on how many detector frequency patterns are available. For the 30 GHz detectors 7 horn patterns at different frequencies inside the bandwidth have been calculated and delivered by ESTEC. The other detectors are only presented by 5 patterns each. The resultant bandpass average patterns are compared with the single frequency patterns by calculating the rms differences in dB inside the regions where the signal to noise levels are large enough for retrieval purpose, see Appendix B.

4.1 LFI27S Main beam pattern

The LFI27S main beams are presented in the output P_{xx} coordinate system calculated from the main beam at the center frequency, 30 GHz. It is defined by the following unit vectors of its x-, y- and z-axis in the FOV coordinate system.

X_axis :	0.921957	-0.379836	0.075634
Y_axis :	0.381256	0.924457	-0.004751
Z_axis :	-0.068115	0.033216	0.997124

or in the GRASP angles

Theta:	4.34619 deg.
Phi:	154.00379 deg.
Psi:	-22.40147 deg.

The horn patterns of the LFI27S detector are delivered at 7 frequencies from 27 GHz to 33 GHz with 1 GHz intervals. The co- and cx-polar differences between the main beams using these detector patterns are seen in Figure 4-2 and Figure 4-3, respectively.

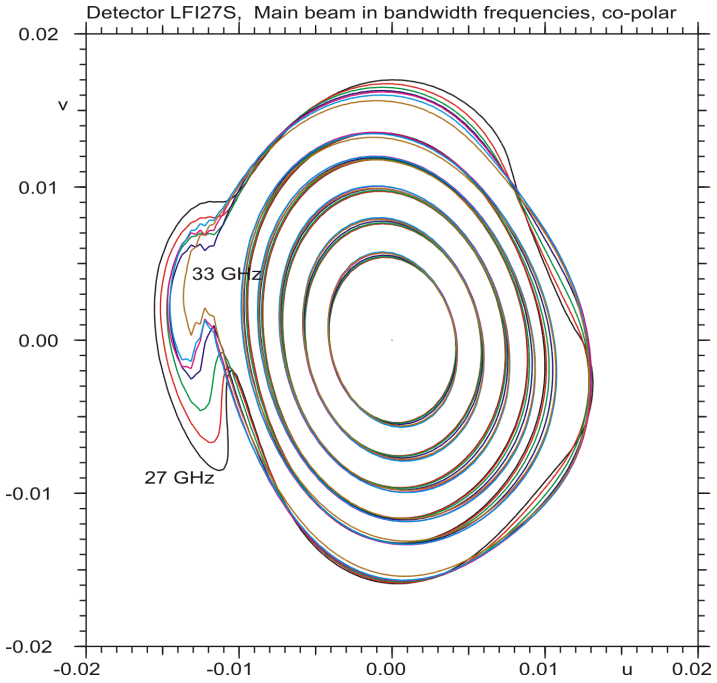

Figure 4-2 Co-polar beams at 7 frequencies from 27 GHz to 33 GHz, down to 30 dB below peak.

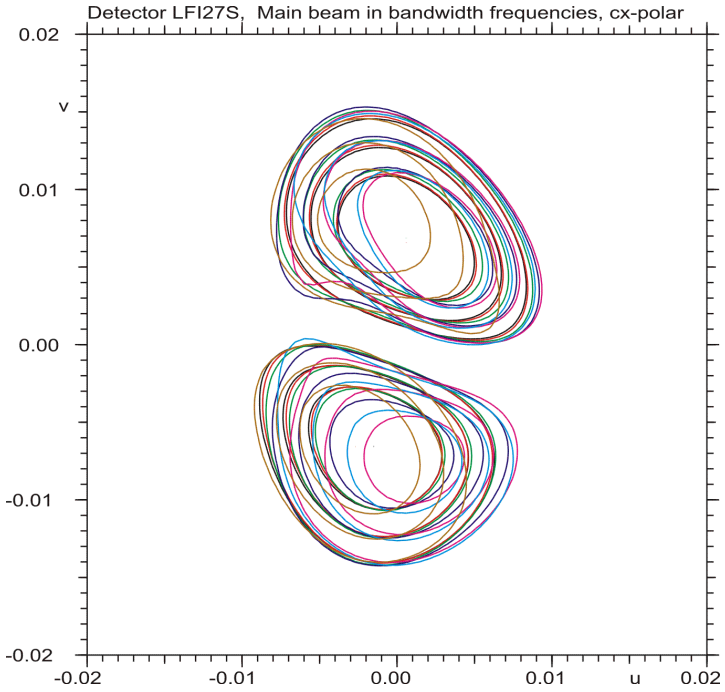

Figure 4-3 Cx-polar pattern at 7 frequencies from 27 GHz to 33 GHz, 3, 6 and 10 dB below peak.

The peaks of the co- and cx-polar field values are given in Table 4-1.

frequency	Co-polar	Cx-polar
GHz	dBi	dBi
27	51.04	23.74
28	51.08	23.31
29	51.05	22.86
30	50.95	22.68
31	50.81	22.89
32	50.79	22.07
33	50.88	22.47

Table 4-1 Co- and Cx-polar peaks.

The averaged radiometer bandshape for the LFI27S detector is found by a summation of the bandpass response values shown in Figure 4-4 in the interval of ±0.5 GHz around the 7 centre frequencies. The average levels are shown as blue lines in the figure.

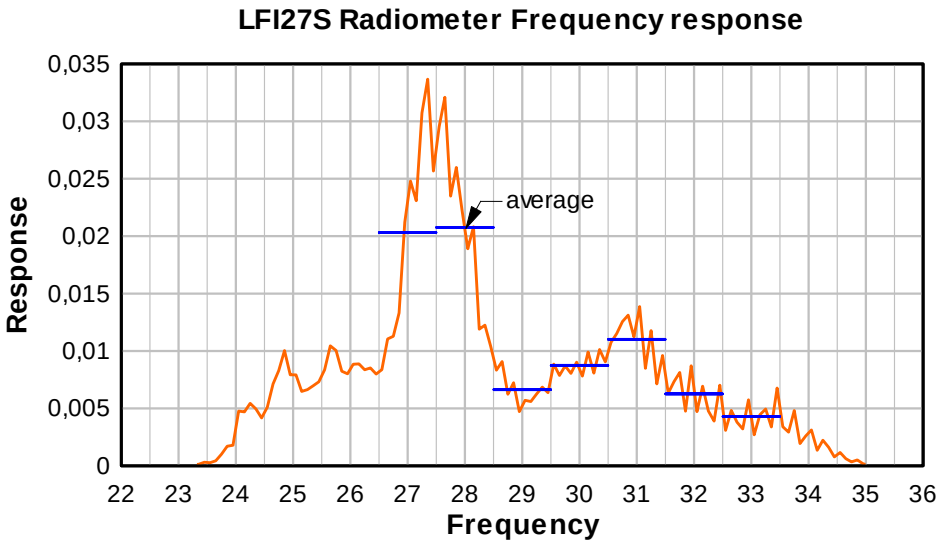

Figure 4-4 7 averaged bandpass responses for detector, LFI27S.

The total bandpass pattern is found by multiplying these average response levels on the individual centre frequency beams and adding these in power, see Figure 4-5.

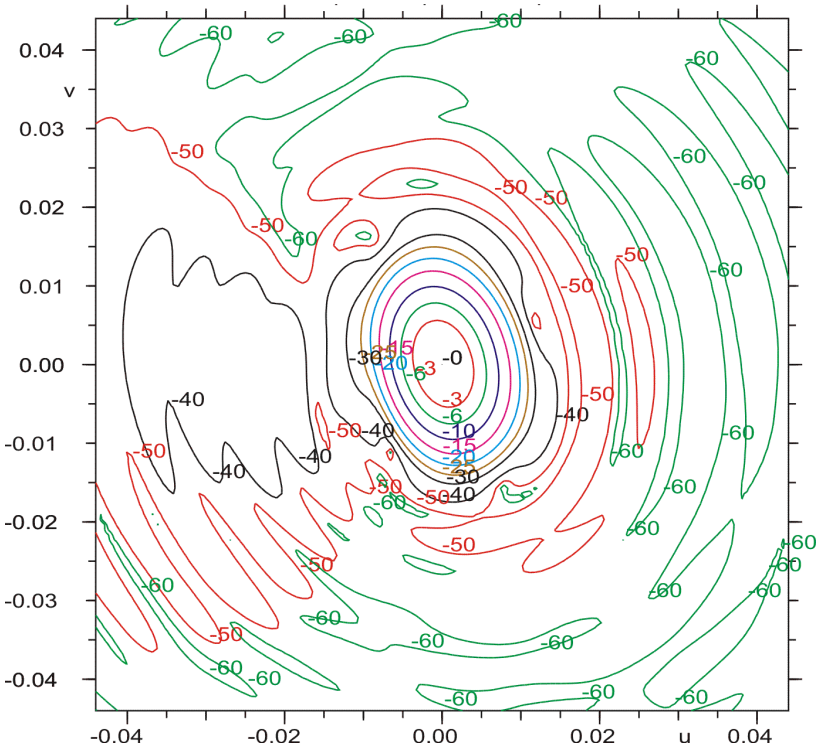

Figure 4-5 Bandpass main beam, detector LFI27S.

In Figure 4-6 the bandpass pattern is shown together with the 28 GHz frequency pattern, which has been used for the LFI27S

detector in the previous retrievals. The two patterns are nearly identical.

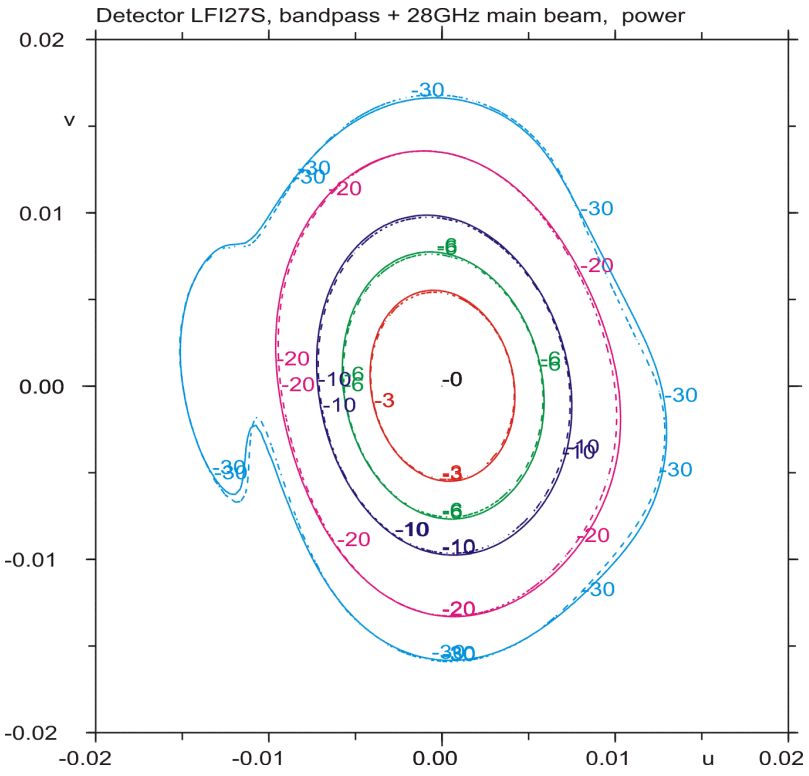

Figure 4-6 Bandpass (full line) & 28 GHz beam (dashed).

The average pattern is compared with the single frequency beams at all the frequencies in Table 4-2, where the deviations are calculated down to different levels.

Rms[dB]	Frequency GHz						
Level	27	28	29	30	31	32	33
12 dB	0.094	0.085	0.041	0.047	0.147	0.184	0.147
20 dB	0.131	0.110	0.045	0.071	0.188	0.222	0.181
30 dB	0.167	0.124	0.056	0.101	0.215	0.249	0.225

Table 4-2 Pattern deviations above the level below peak.

The 29 GHz pattern is the most matching to the average pattern down to 20 dB below peak. Therefore, the detector pattern at 29 GHz may be the best to be used in future retrievals instead of the 28 GHz pattern. On the other hand the bandpass response is also high at the 25 GHz and 26 GHz frequencies, which is not part of the present bandpass calculation. The 29 GHz frequency pattern is shown together with the bandpass pattern in Figure 4-7.

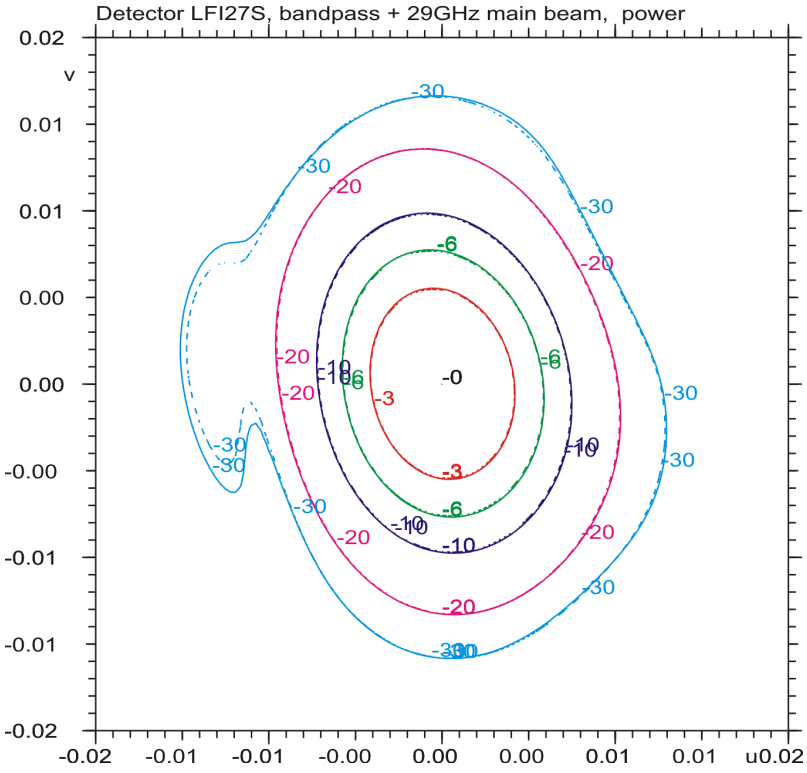

Figure 4-7 Bandpass (full line) & 29 GHz beam (dashed).

4.2 LFI25S Main beam pattern

The LFI25S main beams are presented in the output P_{xx} coordinate system calculated from the main beam at the center frequency, 44 GHz. It is defined by the following unit vectors of its x-, y- and z-axis in the FOV coordinate system.

X_axis :	0.393242	0.915365	-0.086417
Y_axis :	-0.918480	0.395377	0.008437
Z_axis :	0.041890	0.076054	0.996223

or in the GRASP angles

Theta:	4.98114 deg.
Phi:	61.15413 deg.
Psi:	66.73058 deg.

The horn patterns of the LFI25S detector are delivered at 5 frequencies from 39.6 GHz to 48.4 GHz with 2.2 GHz intervals. The co- and cx-polar differences between the main beams using these detector patterns are seen in Figure 4-8 and Figure 4-9, respectively.

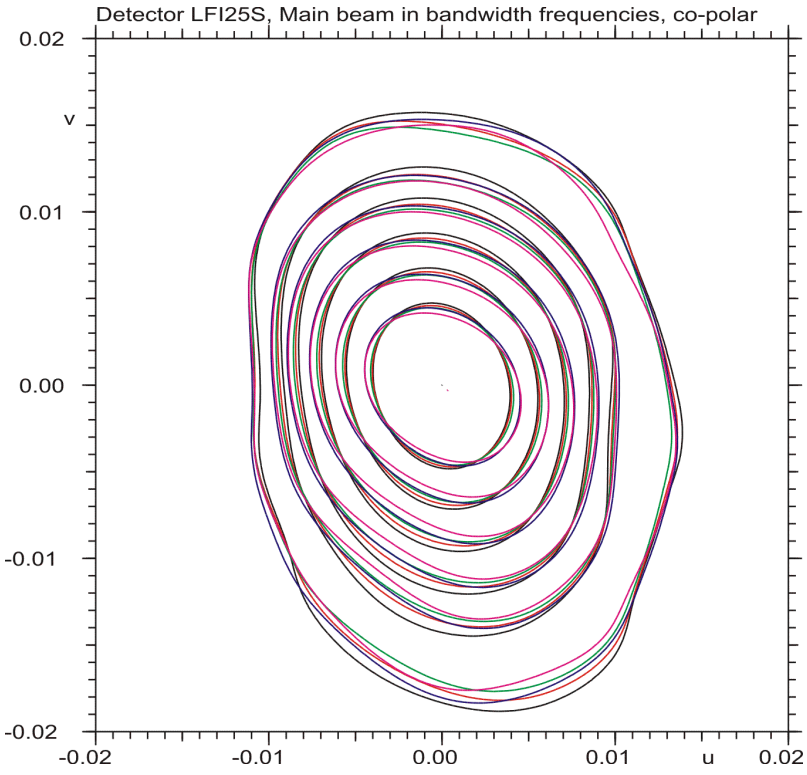

Figure 4-8 Co-polar beams at 5 frequencies from 39.6 GHz to 48.4 GHz, down to 30 dB below peak.

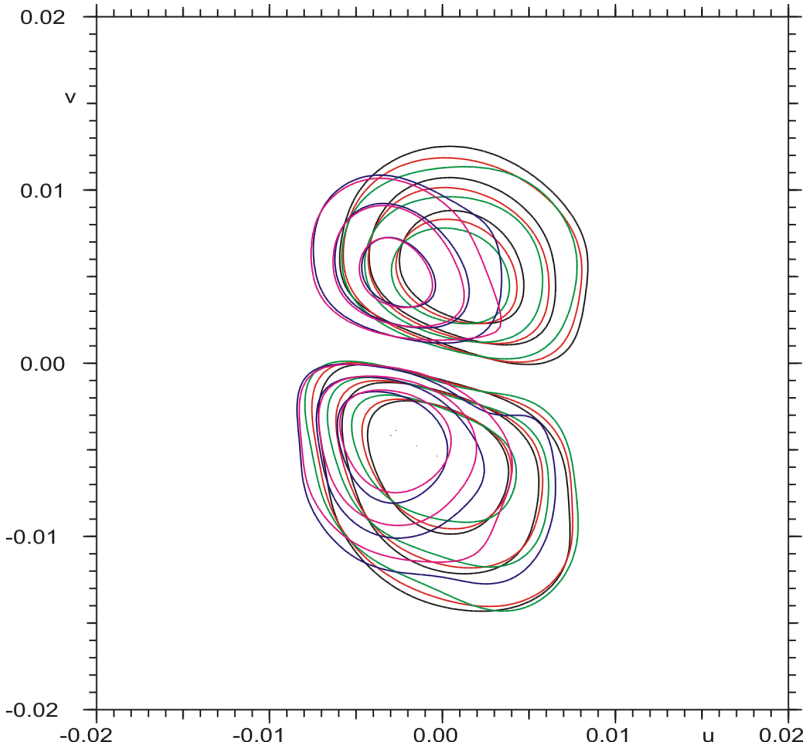

Figure 4-9 Cx-polar pattern at 5 frequencies from 39.6 GHz to 48.4 GHz, 3, 6 and 10 dB below peak.

The peaks of the co- and cx-polar field values are given in Table 4-3

frequency	Co-polar	Cx-polar
GHz	dB	dB
39.6	51.53	27.29
41.8	51.61	26.98
44	51.64	26.78
46.2	51.36	28.60
48.4	51.62	28.23

Table 4-3 Co- and cx-polar peaks.

The average radiometer bandshape for the LFI25S detector is found by a summation of the bandpass response values shown in Figure 4-10 in the interval of ±1.1 GHz around the 5 centre frequencies. The average levels are shown as blue lines in the figure.

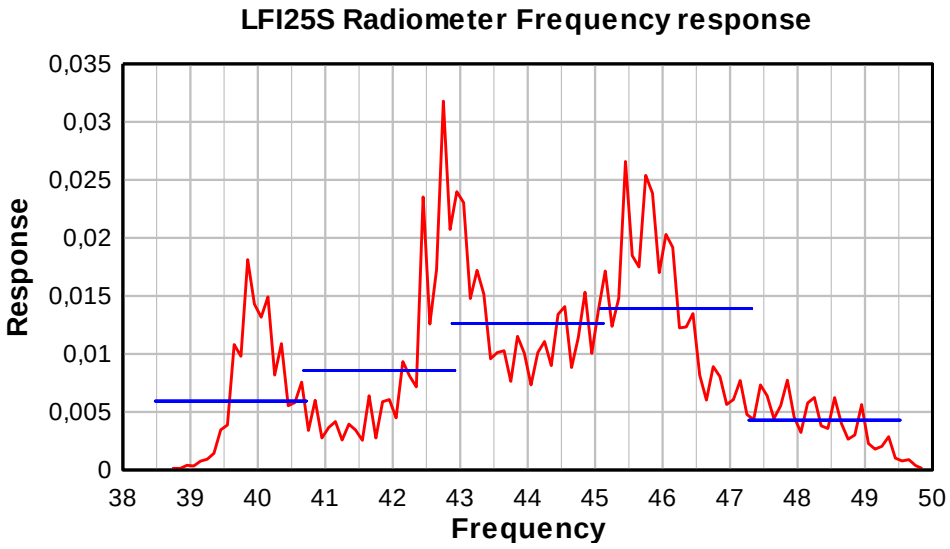

Figure 4-10 5 averaged bandpass responses for detector, LFI25S.

The total bandpass pattern is found by multiplying these average response levels on the individual centre frequency beams and adding these in power, see Figure 4-11.

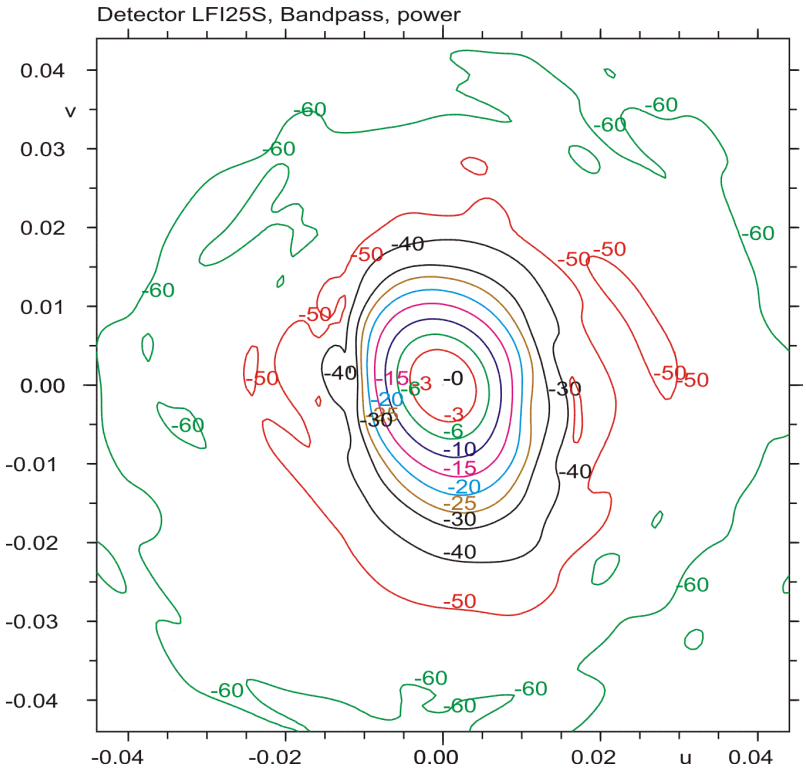

Figure 4-11 Bandpass main beam, detector LFI25S.

In Figure 4-12 the bandpass pattern is shown together with the 44 GHz frequency pattern, which has been used for the LFI25S

detector in the previous retrievals. The two patterns are nearly identical.

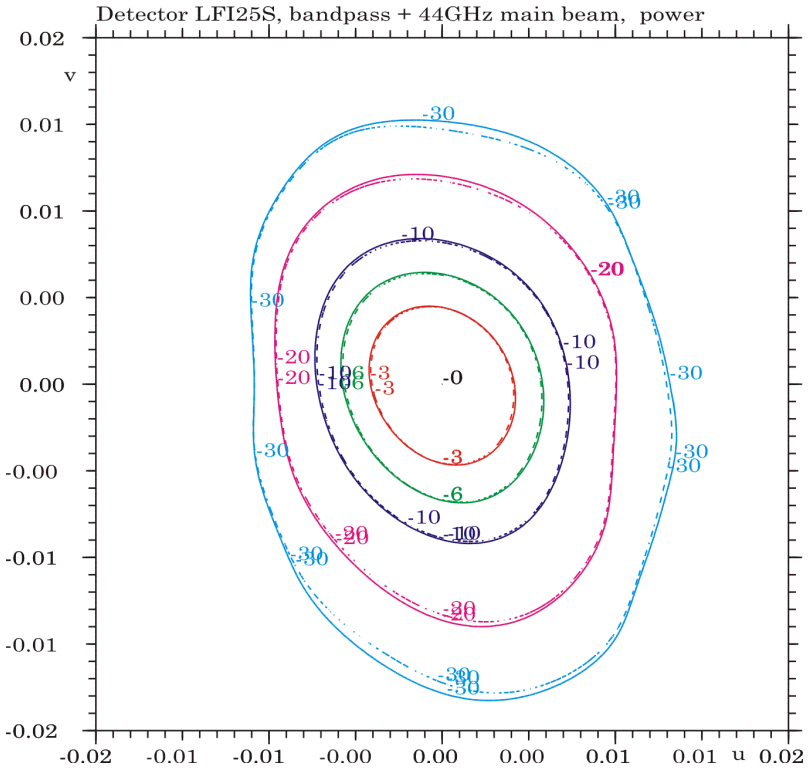

Figure 4-12 Bandpass (full line) & 44 GHz beam (dashed).

The average pattern is compared with the single frequency beams at all the frequencies in Table 4-4 where the deviations are calculated down to different levels.

Rms[dB]	Frequency GHz				
Level	39.6	41.8	44	46.2	48.4
10 dB	0.35	0.20	0.08	0.21	0.38
20 dB	0.44	0.23	0.11	0.24	0.44
30 dB	0.46	0.23	0.12	0.24	0.44

Table 4-4 Pattern deviations above the level below peak.

The 44 GHz pattern is the best match to the average pattern for all levels below peak.

4.3 LFI19S Main beam pattern

The LFI19S main beams are presented in the output P_{xx} coordinate system calculated from the main beam at the center frequency, 70 GHz. It is defined by the following unit vectors of its x-, y- and z-axis in the FOV coordinate system.

X_axis :	0.923646	0.379196	0.055566
Y_axis :	-0.380135	0.924905	0.007011
Z_axis :	-0.048735	-0.027598	0.998430

or in the GRASP angles

Theta:	3.21062 deg.
Phi:	-150.47734 deg.
Psi:	22.33144 deg.

The horn patterns of the LFI19S detector are delivered at 5 frequencies, 63 GHz, 66 GHz, 70 GHz, 74 GHz and 77 GHz. The co- and cx-polar differences between the main beams using these detector patterns are seen in Figure 4-13 and Figure 4-14, respectively.

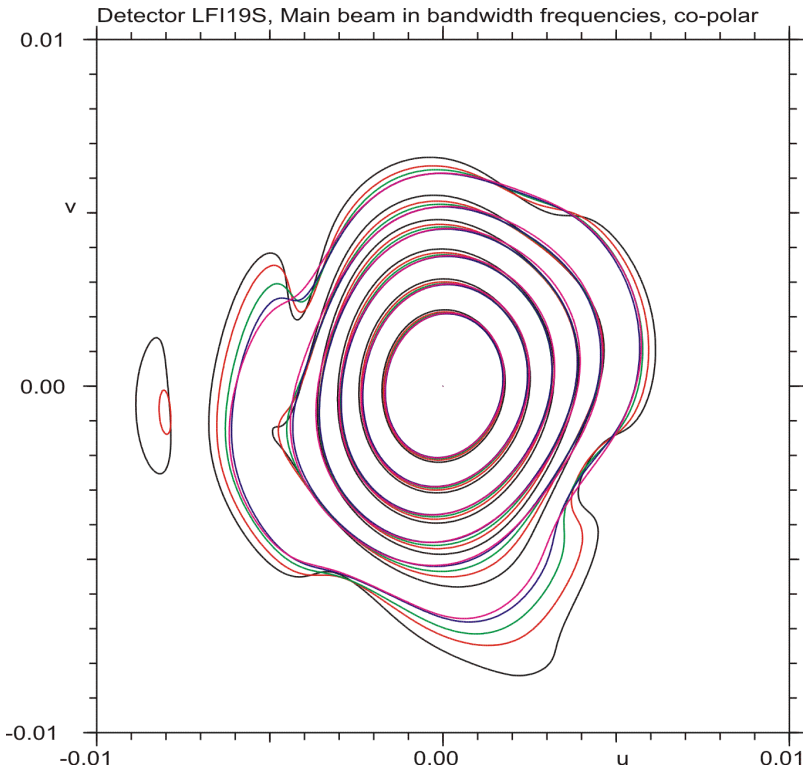

Figure 4-13 Co-polar beams at 5 frequencies from 63 GHz to 77 GHz, down to 30 dB below peak.

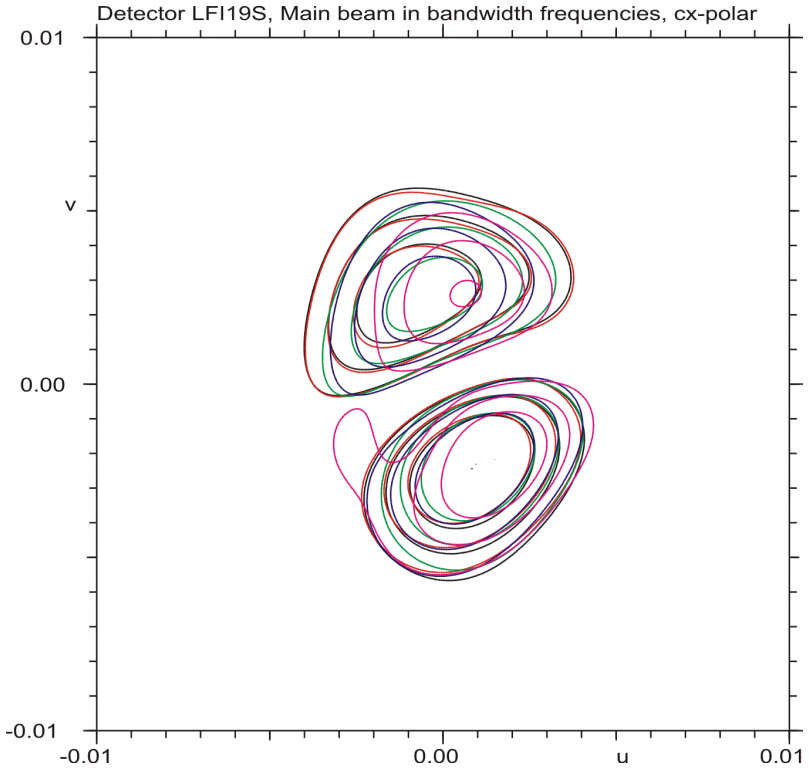

Figure 4-14 Cx-polar pattern at 5 frequencies from 63 GHz to 77 GHz, 3, 6 and 10 dB below peak.

The peaks of the co- and cx-polar field values are given in Table 4-5

frequency	Co-polar	Cx-polar
GHz	dB	dB
63	58.56	29.23
66	58.80	29.18
70	58.96	29.22
74	59.06	28.51
77	58.96	29.68

Table 4-5 Co- and cx-polar peaks.

The averaged radiometer bandshape for the LFI19S detector is found by a summation of the bandpass response values shown in Figure 4-15 in the interval of ±1.5 GHz around the 5 centre frequencies. The average levels are shown as blue lines in the figure.

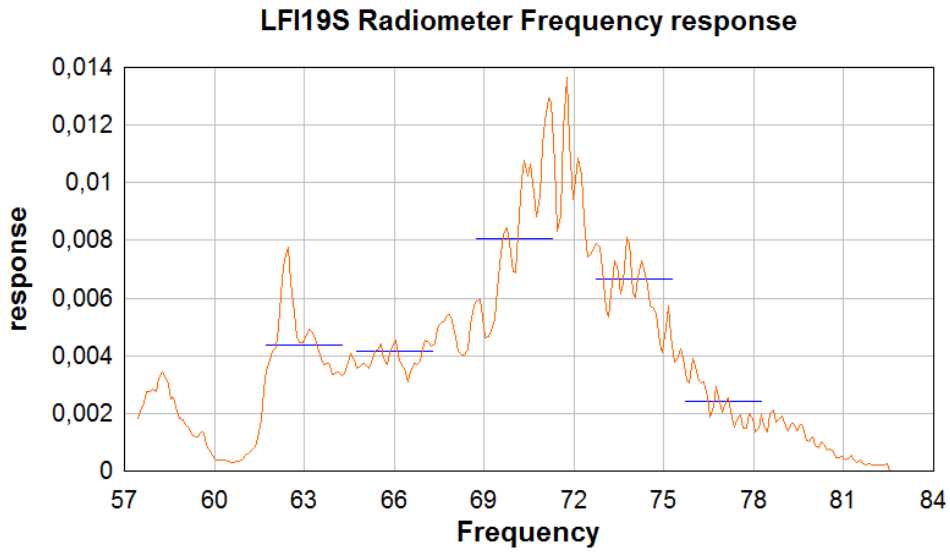

Figure 4-15 5 averaged bandpass responses for detector, LFI19S.

The total bandpass pattern is found by multiplying these average response levels on the individual centre frequency beams and adding these in power, see Figure 4-16.

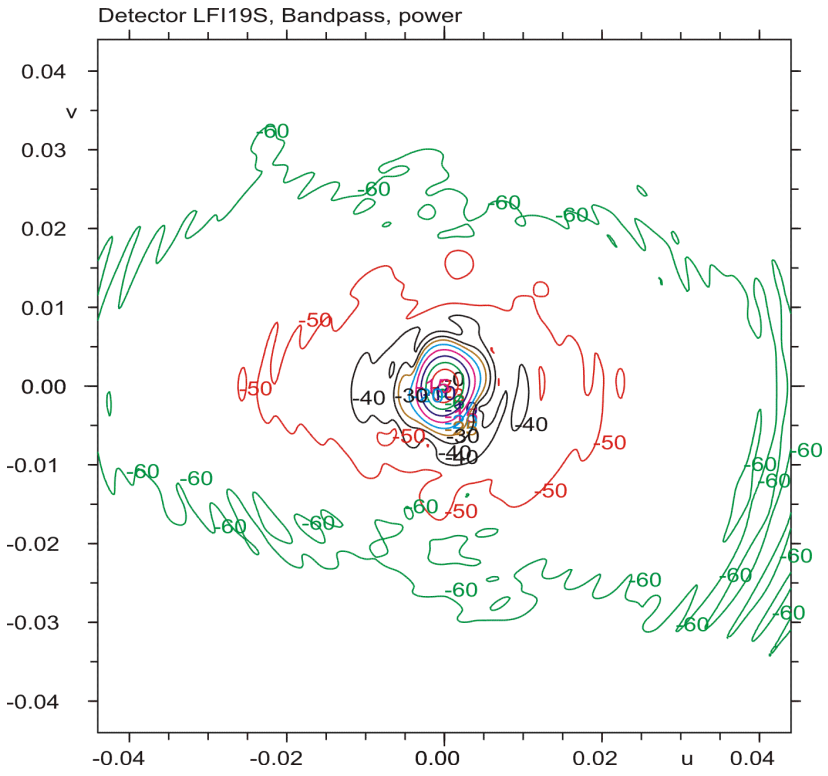

Figure 4-16 Bandpass main beam, detector LFI19S.

In Figure 4-17 the bandpass pattern is shown together with the 70 GHz frequency pattern, which has been used for the LFI19S detector in the previous retrievals. The two patterns are nearly identical.

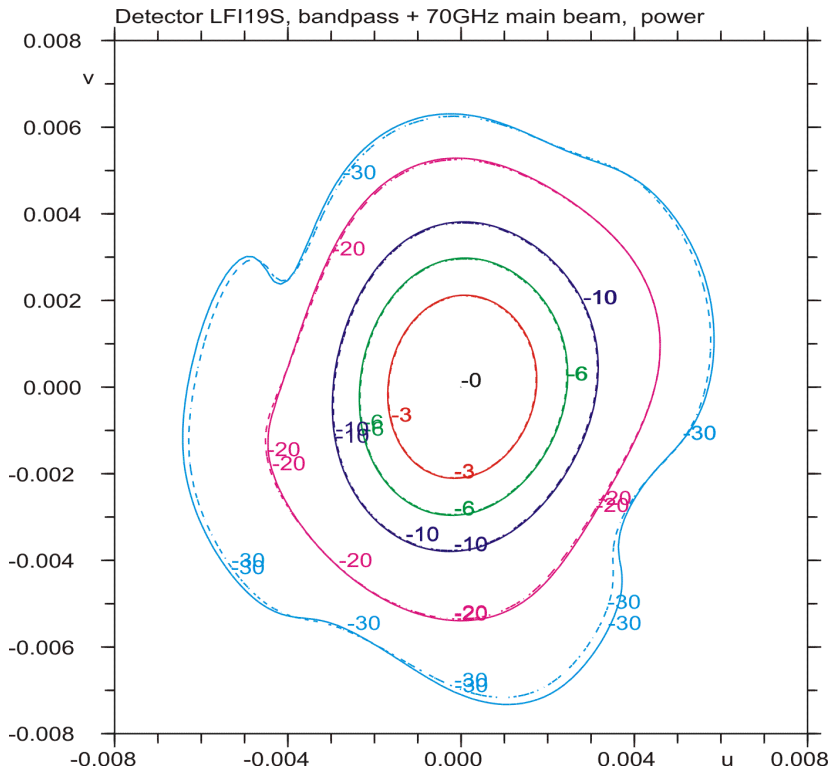

Figure 4-17 Bandpass (full line) & 70 GHz beam (dashed).

The average pattern is compared with the single frequency beams at all the frequencies in Table 4-6 where the deviations are calculated down to different levels.

Rms[dB]	Frequency GHz				
Level	63	66	70	74	77
10 dB	0.19	0.07	0.04	0.10	0.12
20 dB	0.26	0.09	0.05	0.15	0.19
30 dB	0.32	0.12	0.07	0.20	0.26

Table 4-6 Pattern deviations above the level below peak.

The 70 GHz pattern is the best match to the average pattern for all levels below peak.

5. HFI bandpasses.

In this Chapter the HFI bandpasses delivered from ESTEC are used to simulate the influence on the main beams measured. All the radiometer bandshapes are shown in Figure 5-1.

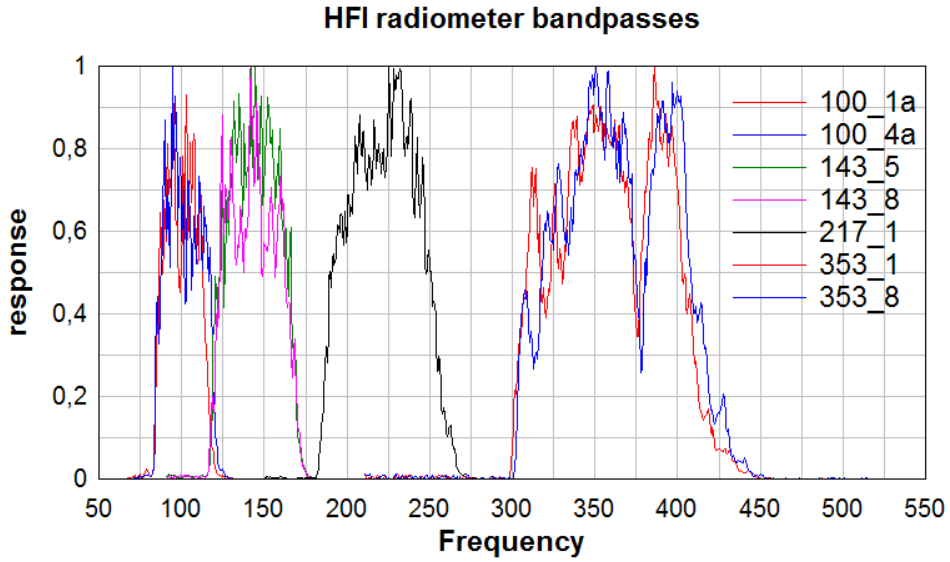

Figure 5-1 HFI bandpasses.

The radiometer bandshapes in Figure 5-1 have to be averaged in different frequency intervals at the 5 detector frequency patterns available. The resultant bandpass average patterns are compared with the single frequency patterns by calculating the rms differences in dB inside the regions where the signal to noise levels are large enough for retrieval purposes, see Appendix B.

5.1 HFI_100_3a Main beam pattern

The HFI_100_3a main beams are presented in the output P_{xx} coordinate system calculated from the main beam at the center frequency, 100 GHz. It is defined by the following unit vectors of its x-, y- and z-axis in the FOV coordinate system.

X_axis :	0.999514	-0.000232	0.031162
Y_axis :	0.000423	0.999981	-0.006124
Z_axis :	-0.031160	0.006134	0.999496

or in the GRASP angles

Theta:	1.81990 deg.
Phi:	168.86284 deg.
Psi:	-0.01878 deg.

The horn patterns of the HFI_100_3a detector are delivered at 5 frequencies, 85 GHz, 92 GHz, 100 GHz, 108 GHz and 116 GHz. The co- and cx-polar differences between the main beams using these detector patterns are seen in Figure 5-2 and Figure 5-3, respectively.

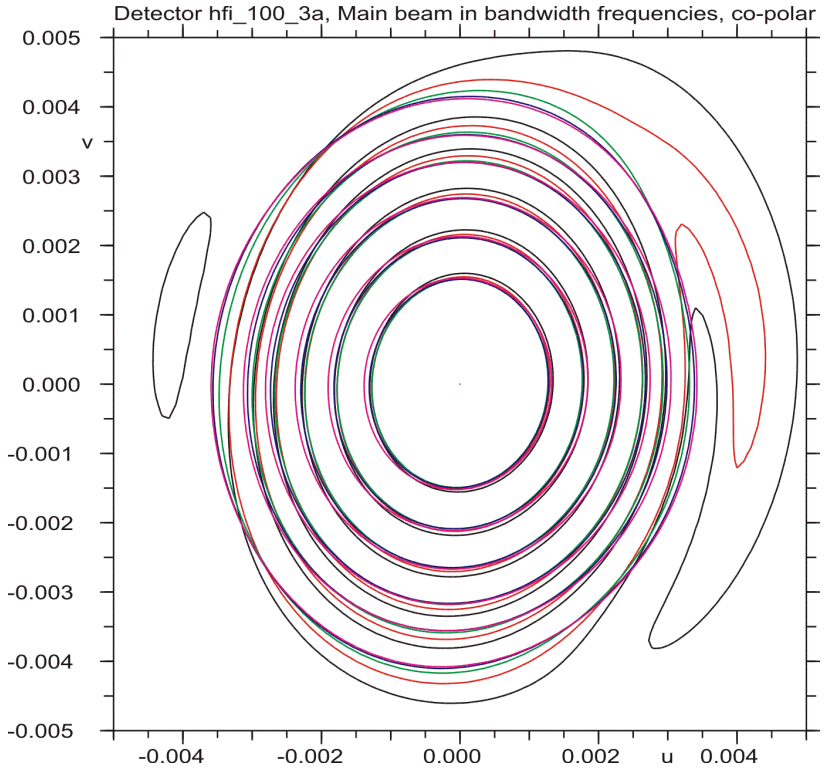

Figure 5-2 Co-polar main beams at 5 frequencies from 85 GHz to 116 GHz, detector HFI_100_3a.

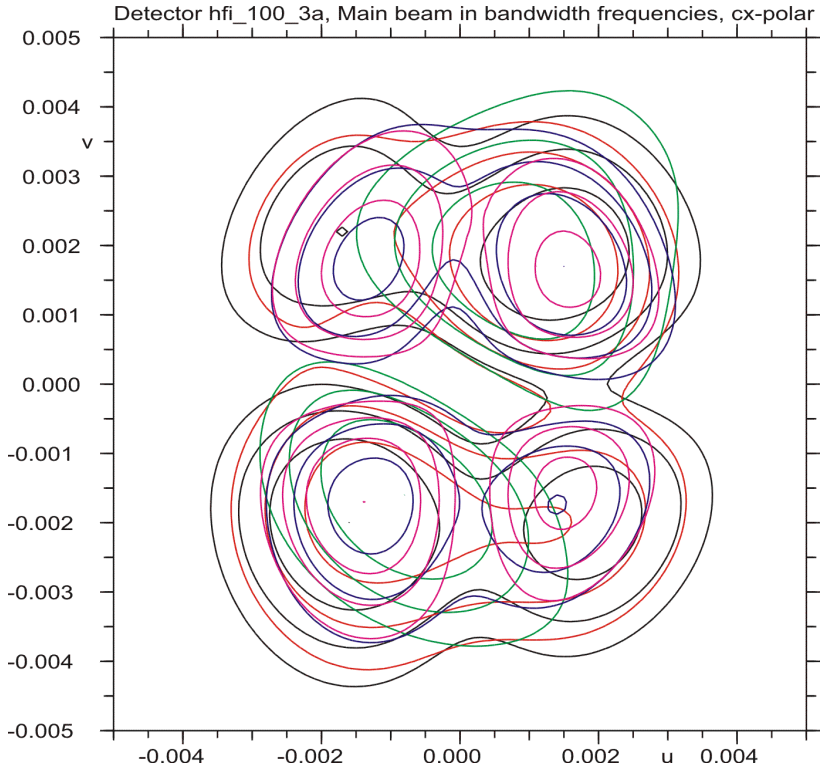

Figure 5-3 Cx-polar pattern at 5 frequencies from 85 GHz to 116 GHz, 3, 6 and 10 dB below peak.

The peaks of the co- and cx-polar field values are given in Table 5-1.

frequency	Co-polar	Cx-polar
GHz	dB	dB
85	61.40	25.83
92	61.69	23.87
100	61.81	22.04
108	61.73	25.55
116	61.53	29.67

Table 5-1 Co- and cx-polar peaks.

The averaged radiometer bandshape for the HFI-100-3a detector is found by a summation of the bandpass response values shown in Figure 5-4 in the interval of ±3.5 GHz around the 5 centre frequencies. The average levels are shown as blue lines in the figure.

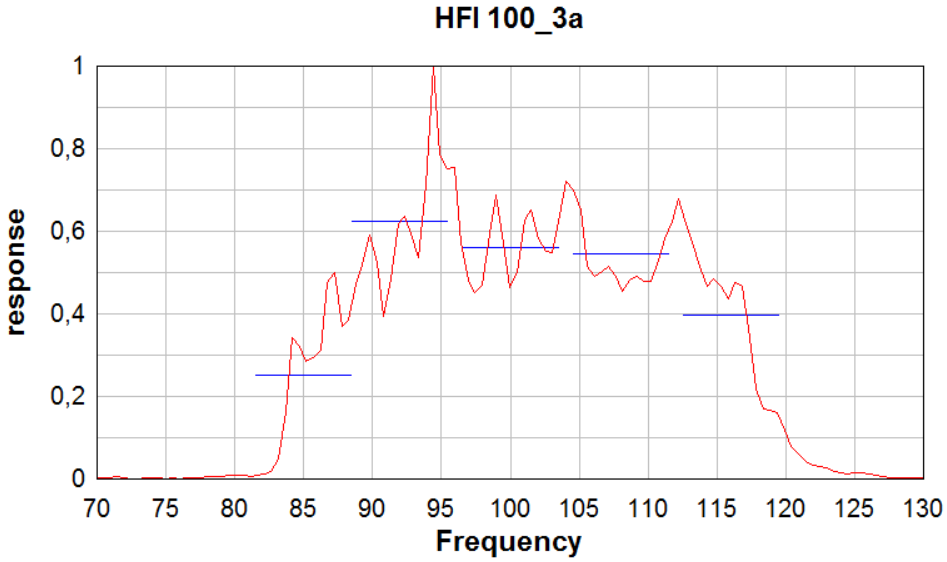

Figure 5-4 5 averaged bandpass responses for detector, HFI-100-3a.

The total bandpass pattern is found by multiplying these average response levels on the individual centre frequency beams and adding these in power, see Figure 5-5.

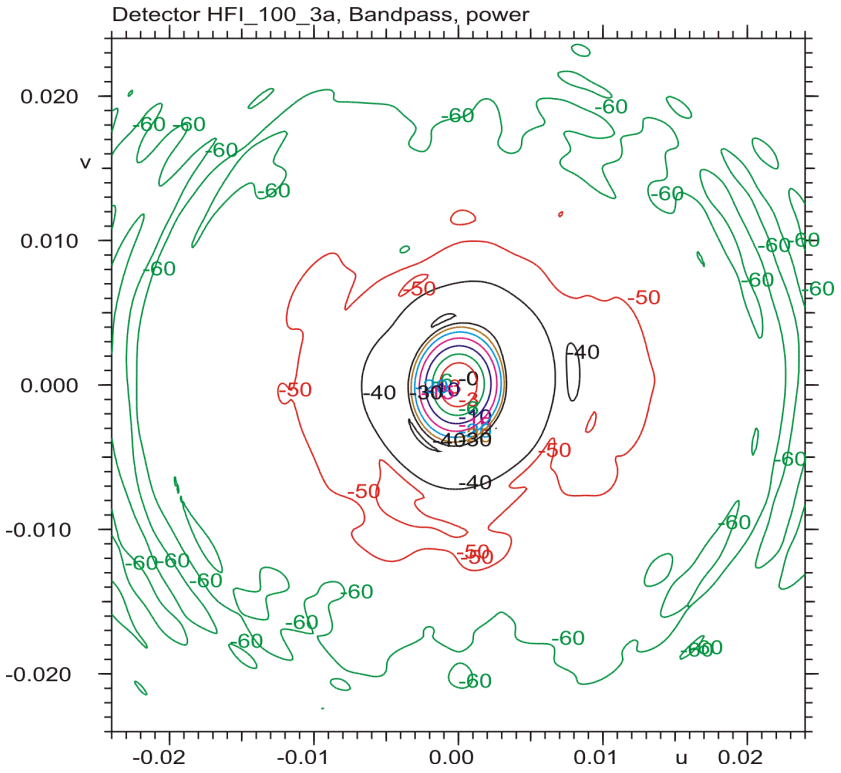

Figure 5-5 Bandpass main beam, detector HFI_100_3a.

In Figure 5-6 the bandpass pattern is shown together with the 100 GHz frequency pattern, which has been used for the HFI_100_3a detector in the previous retrievals. The two patterns are nearly identical.

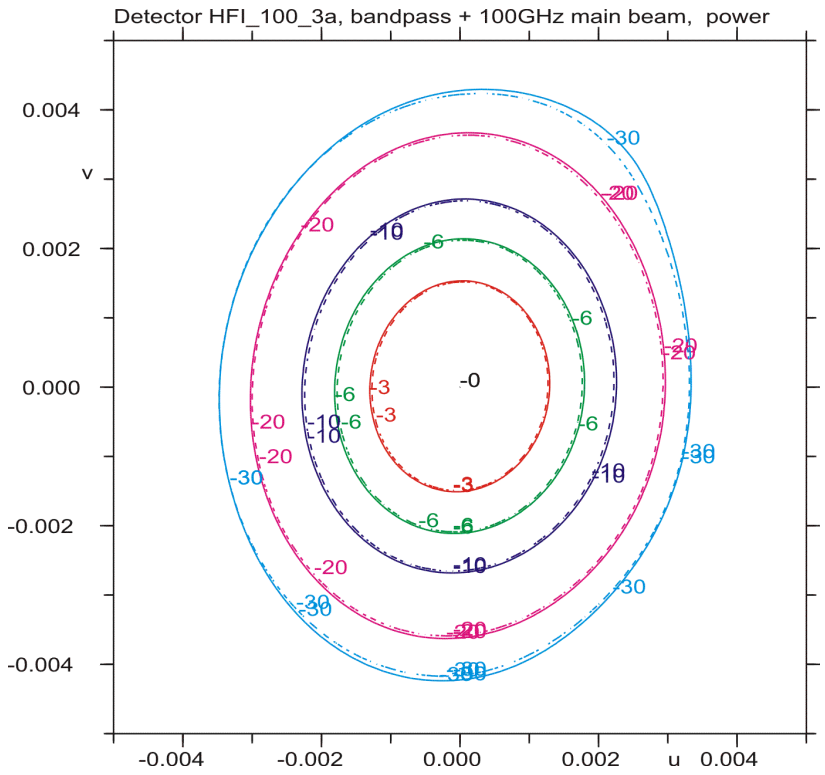

Figure 5-6 Bandpass (full line) & 100 GHz beam (dashed).

The average pattern is compared with the single frequency beams at all the frequencies in Table 5-2 where the deviations are calculated down to different levels.

Rms[dB]	Frequency GHz				
Level	85	92	100	108	116
10 dB	0.17	0.08	0.08	0.06	0.17
20 dB	0.24	0.13	0.11	0.10	0.23

Table 5-2 Pattern deviations above the level below peak.

The 100 GHz and the 108 GHz patterns are the best match to the average pattern for all levels below peak.

5.2 HFI_143_2a Main beam pattern

The HFI_143_2a main beams are presented in the output P_{xx} coordinate system calculated from the main beam at the center frequency, 143 GHz. It is defined by the following unit vectors of its x-, y- and z-axis in the FOV coordinate system.

X_axis :	0.706718	0.707454	-0.007605
Y_axis :	-0.707175	0.706681	0.022507
Z_axis :	0.021297	-0.010528	0.999718

or in the GRASP angles

Theta:	1.36128 deg.
Phi:	-26.30480 deg.
Psi:	45.02492 deg.

The horn patterns of the HFI_143_2a detector are delivered at 5 frequencies, 121 GHz, 132 GHz, 143 GHz, 155 GHz and 166 GHz. The co- and cx-polar differences between the main beams using these detector patterns are seen in Figure 5-7 and Figure 5-8, respectively.

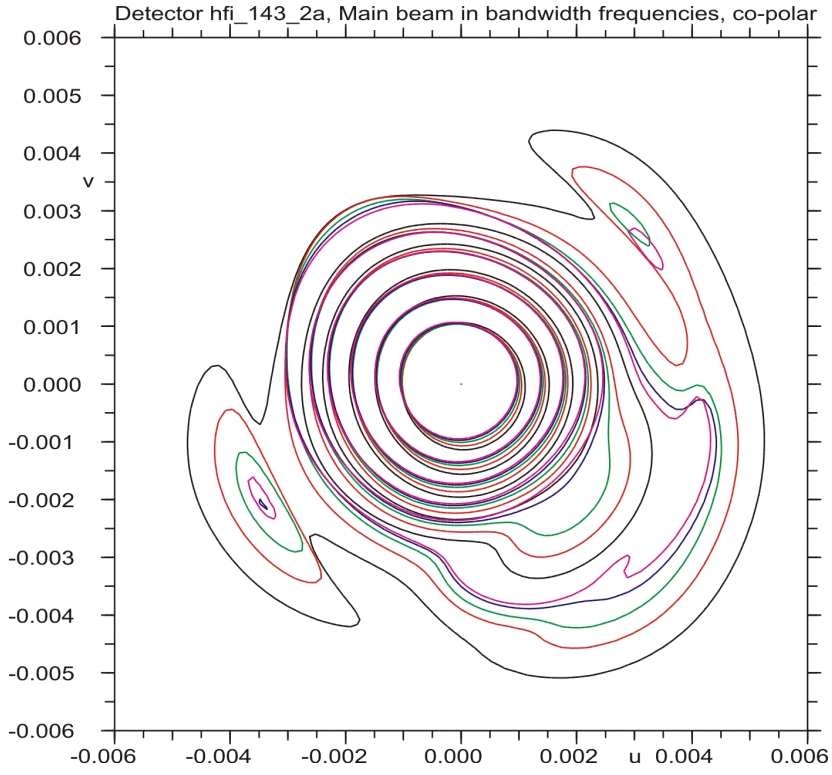

Figure 5-7 Co-polar main beams at 5 frequencies from 121 GHz to 166 GHz, detector HFI_143_2a.

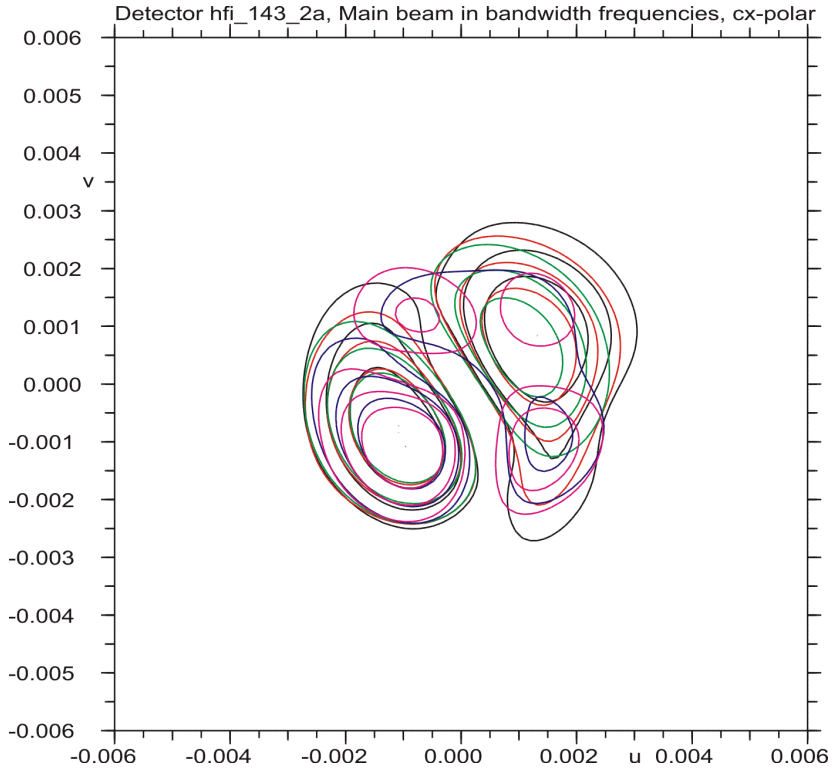

Figure 5-8 Cx-polar pattern at 5 frequencies from 121 GHz to 166 GHz, 3, 6 and 10 dB below peak.

The peaks of the co- and cx-polar field values are given in Table 5-1.

frequency	Co-polar	Cx-polar
GHz	dB	dB
121	63.61	34.20
132	64.01	33.71
143	64.23	33.26
155	64.33	35.10
166	64.36	36.98

Table 5-3 Co- and cx-polar peaks.

The averaged radiometer bandshape for the HFI-143-2a detector is found by a summation of the bandpass response values shown in Figure 5-9 in the interval of ±5.5 GHz around the 5 centre frequencies. The average levels are shown as blue lines in the figure.

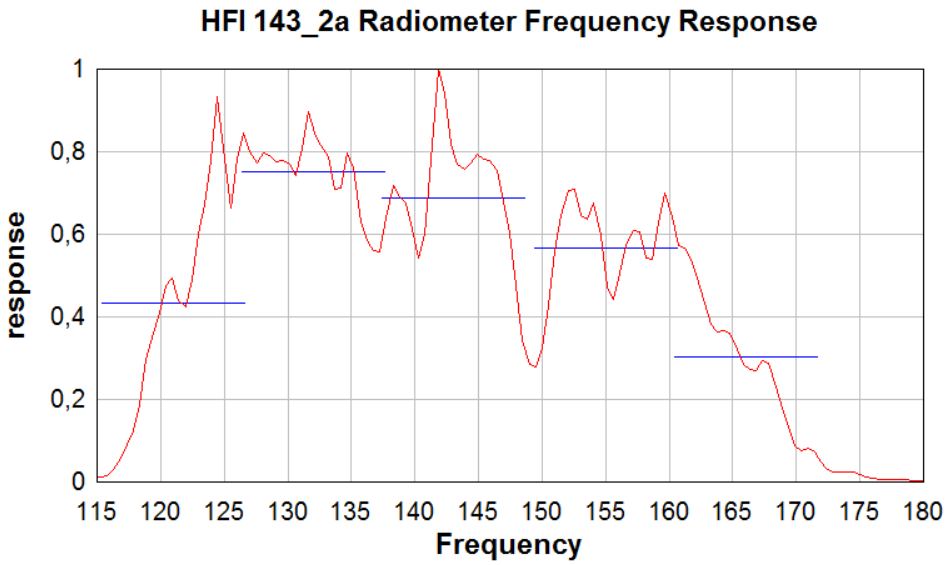

Figure 5-9 5 averaged bandpass responses for detector, HFI-143-2a.

The total bandpass pattern is found by multiplying these average response levels on the individual centre frequency beams and adding these in power, see Figure 5-10.

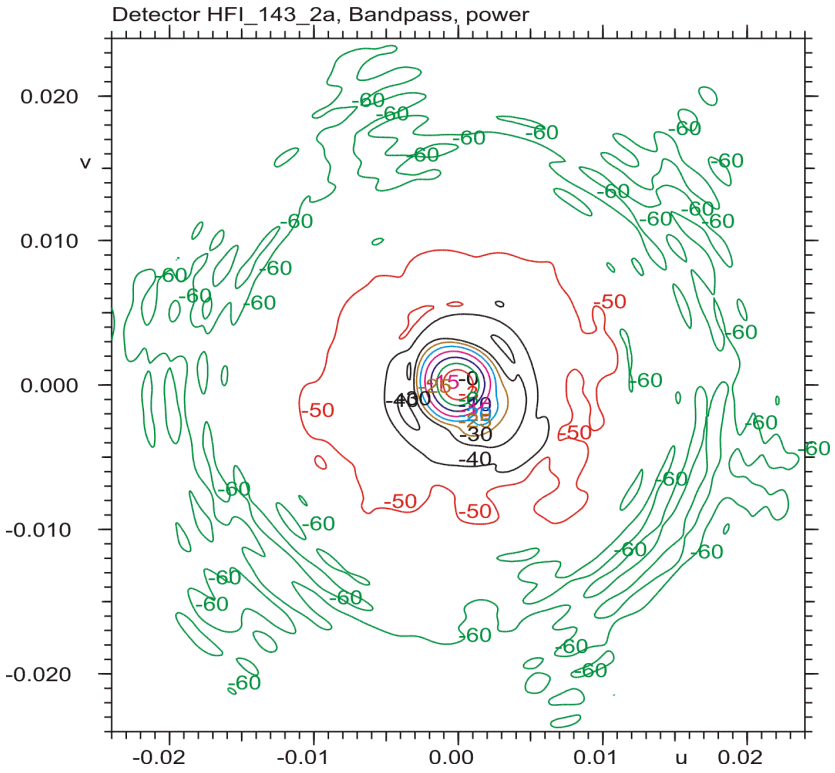

Figure 5-10 Bandpass main beam, detector HFI_143_2a.

In Figure 5-11 the bandpass pattern is shown together with the 143 GHz frequency pattern, which has been used for the HFI_143_2a detector in the previous retrievals. The difference between the two patterns is not very large, but differences can be observed around -20 dB.

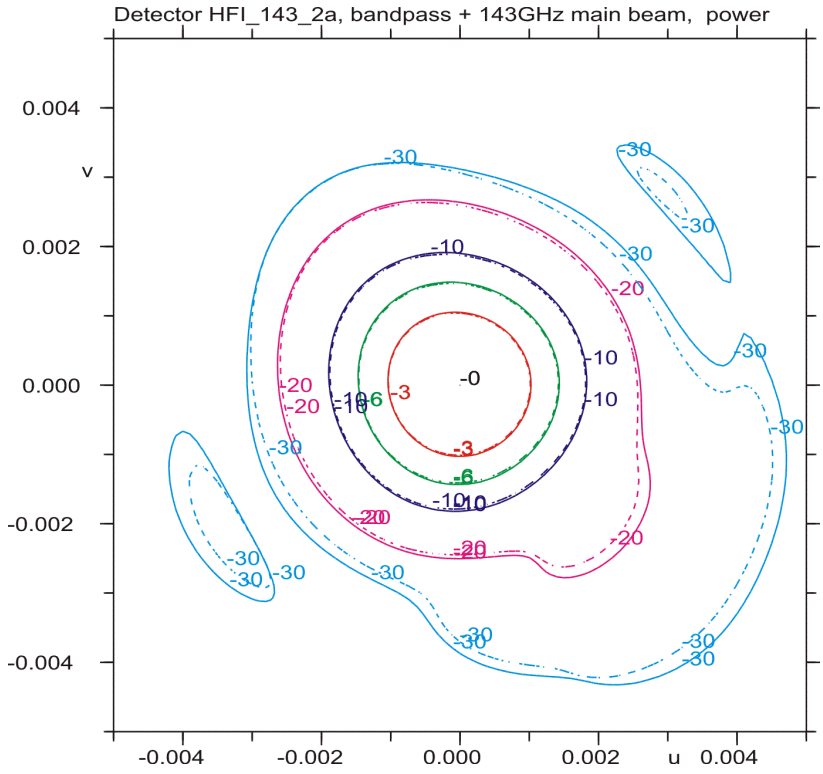

Figure 5-11 Bandpass (solid line) & 143 GHz beam (dashed).

The average pattern is compared with the single frequency beams at all the frequencies in Table 5-4 where the deviations are calculated down to different levels.

Rms[dB]	Frequency GHz				
Level	121	132	143	155	166
10 dB	0.34	0.14	0.07	0.21	0.32
20 dB	0.49	0.18	0.12	0.33	0.49

Table 5-4 Pattern deviations above level below peak.

The 143 GHz pattern is the best match to the average pattern for all levels below peak.

5.3 HFI_217_6a Main beam pattern

The HFI_217_6a main beams are presented in the output P_{xx} co-ordinate system calculated from the main beam at the center frequency, 217 GHz. It is defined by the following unit vectors of its x-, y- and z-axis in the FOV coordinate system.

X_axis :	0.708182	0.705910	0.013033
Y_axis :	-0.705981	0.708229	0.001301
Z_axis :	-0.008312	-0.010122	0.999914

or in the GRASP angles

Theta:	0.75048 deg.
Phi:	-129.39173 deg.
Psi:	44.90845 deg.

The horn patterns of the HFI_217_6a detector are delivered at 5 frequencies, 193 GHz, 205 GHz, 217 GHz, 235 GHz and 252 GHz. The co- and cx-polar differences between the main beams using these detector patterns are seen in Figure 5-12 and Figure 5-13, respectively.

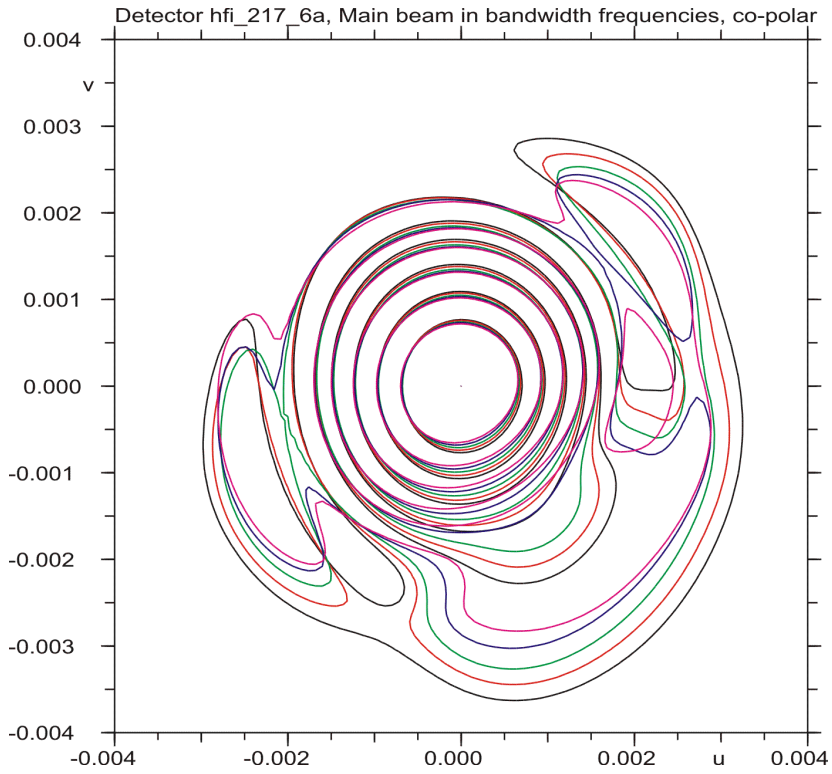

Figure 5-12 Co-polar main beams at 5 frequencies from 193 GHz to 252 GHz, detector HFI_217_6a.

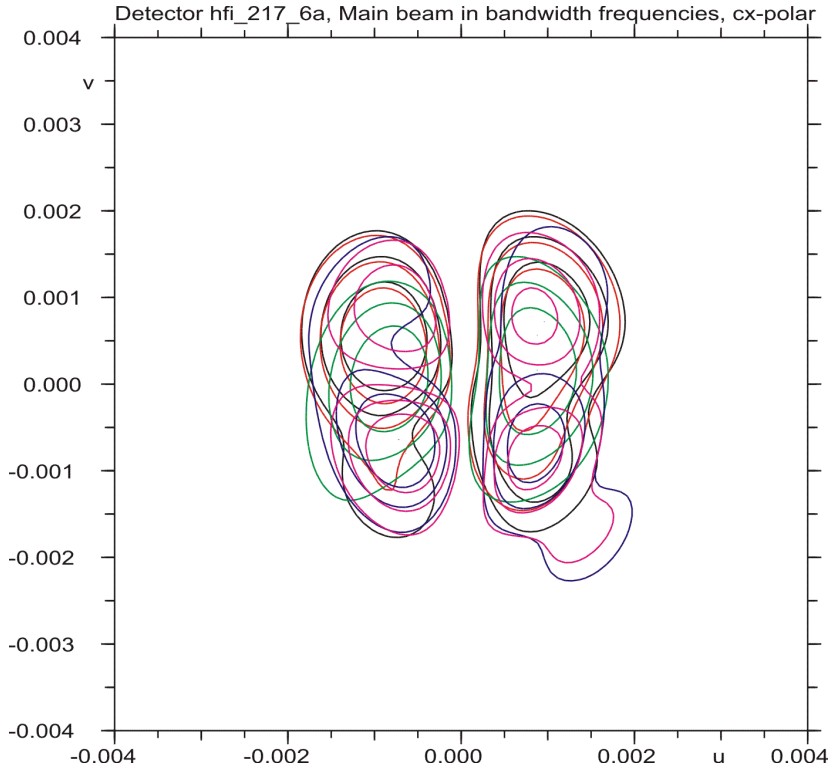

Figure 5-13 Cx-polar pattern at 5 frequencies from 193 GHz to 252 GHz, 3, 6 and 10 dB below peak.

The peaks of the co- and cx-polar field values are given in Table 5-5

frequency	Co-polar	Cx-polar
GHz	dB	dB
193	67.17	30.65
205	67.35	28.75
217	67.57	27.27
235	67.71	28.66
252	67.79	32.31

Table 5-5 Co- and cx-polar peaks.

The averaged radiometer bandshape for the HFI-217-6a detector is found by a summation of the bandpass response values shown in Figure 5-14 in the interval of ±5.5 GHz around the center frequencies. The average levels are shown as blue lines in the figure.

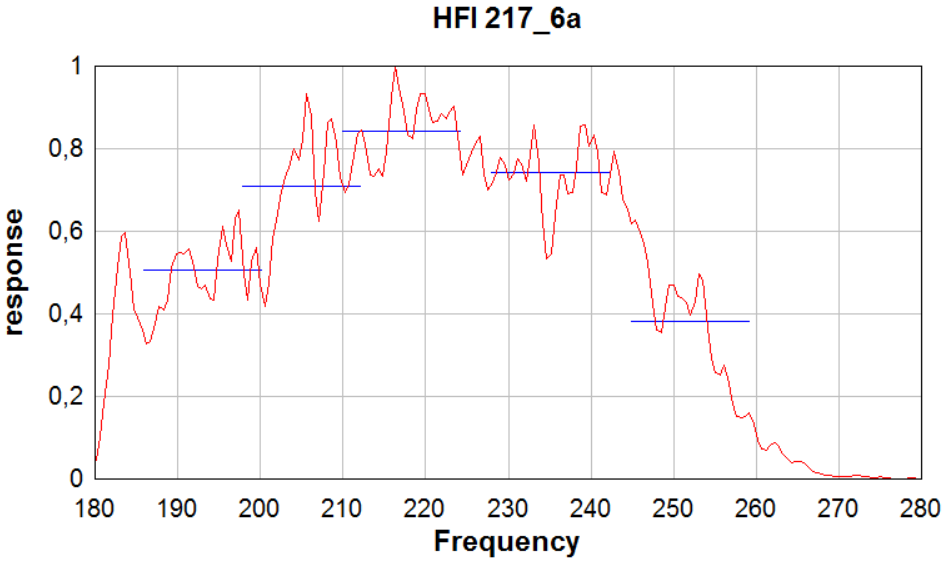

Figure 5-14 5 averaged bandpass responses for detector, HFI-217-6a.

The total bandpass pattern is found by multiplying these average response levels on the individual centre frequency beams and adding these in power, see Figure 5-15.

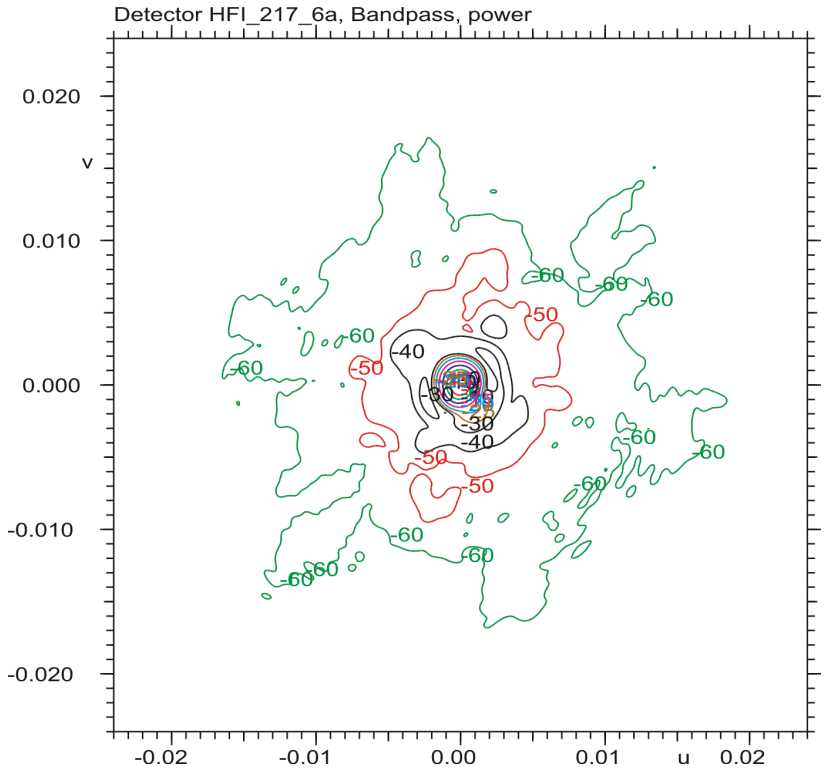

Figure 5-15 Bandpass main beam, detector HFI_217_6a.

In Figure 5-16 the bandpass pattern is shown together with the 217 GHz frequency pattern, which has been used for the HFI_217_6a detector in the previous retrievals. The two patterns are nearly identical.

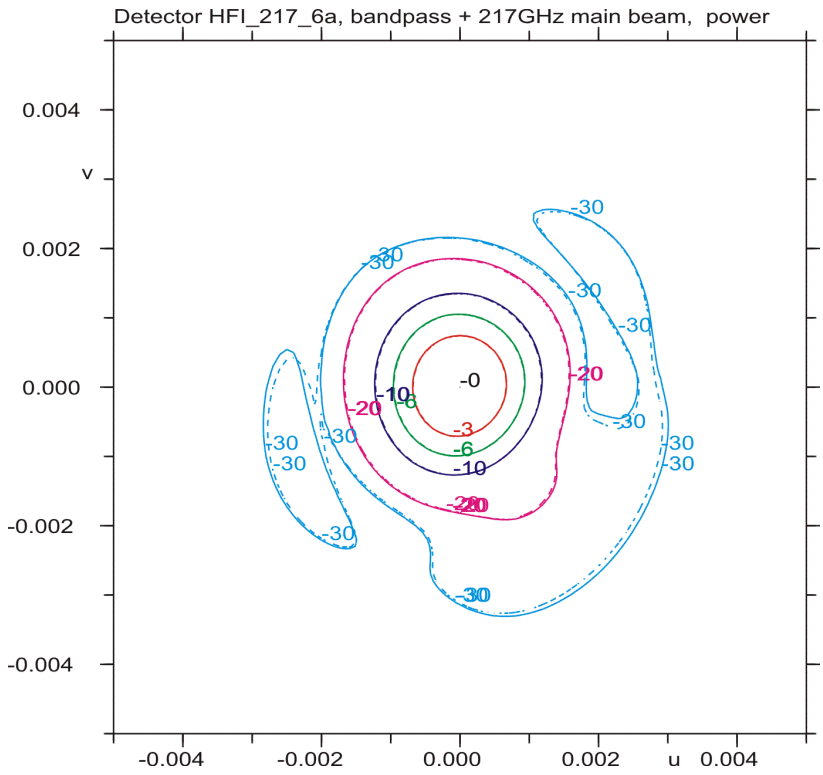

Figure 5-16 Bandpass (solid line) & 217 GHz beam (dashed).

The average pattern is compared with the single frequency beams at all the frequencies in Table 5-6, where the deviations are calculated down to different levels.

Rms[dB]	Frequency GHz				
Level	193	205	217	235	252
10 dB	0.26	0.14	0.04	0.16	0.33
20 dB	0.38	0.20	0.06	0.29	0.58

Table 5-6 Pattern deviations above level below peak.

The 217 GHz patterns is the best match to the average pattern for all levels below peak.

5.4 HFI_353_5b Main beam pattern

The HFI_353_5b main beams are presented in the output P_{xx} coordinate system calculated from the main beam at the center frequency, 353 GHz. It is defined by the following unit vectors of its x-, y- and z-axis in the FOV coordinate system.

X_axis :	0.009919	-0.999933	0.005887
Y_axis :	0.999951	0.009918	-0.00025
Z_axis :	0.000187	0.005889	0.999983

or in the GRASP angles

Theta:	0.33760 deg.
Phi:	88.18058 deg.
Psi:	-89.43169 deg.

The horn patterns of the HFI_353_5b detector are delivered at 5 frequencies, 315 GHz, 334 GHz, 353 GHz, 382 GHz and 410 GHz The co- and cx-polar differences between the main beams using these detector patterns are seen in Figure 5-17 and Figure 5-18, respectively.

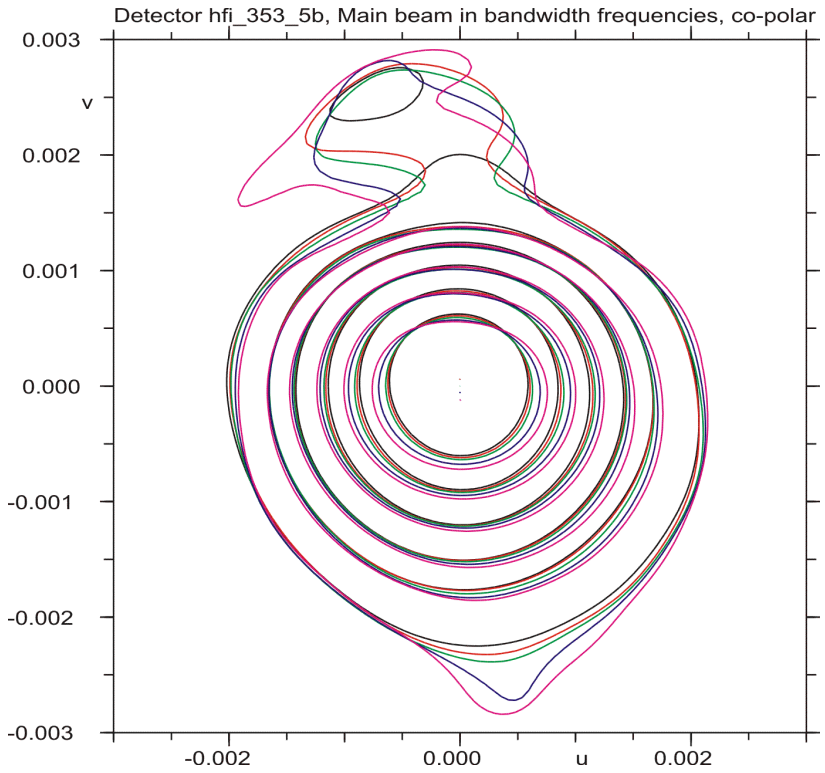

Figure 5-17 Co-polar main beams at 5 frequencies from 315 GHz to 410 GHz, detector HFI_353_5b.

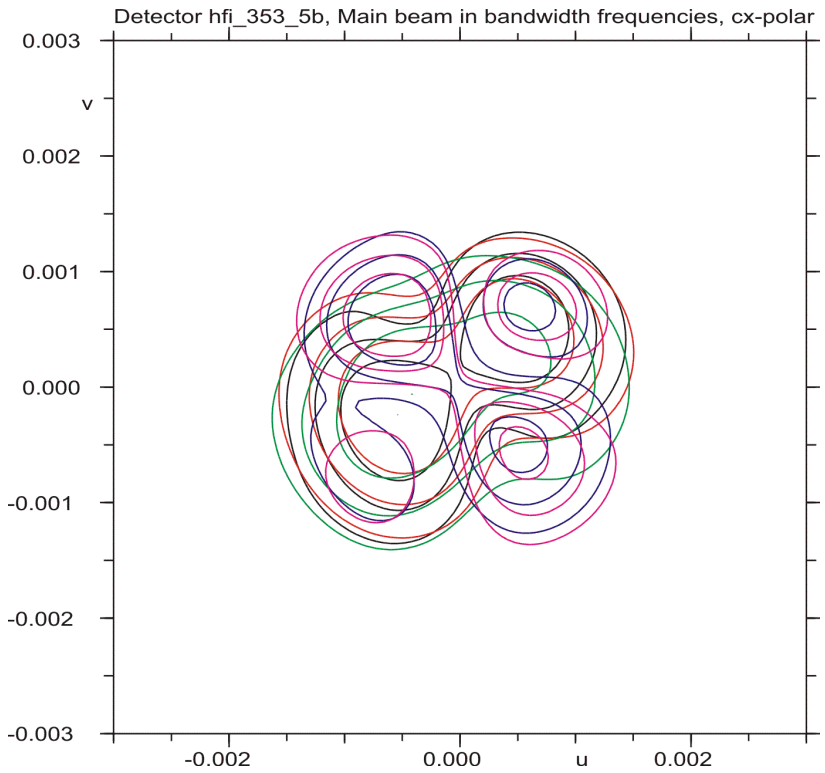

Figure 5-18 Cx-polar pattern at 5 frequencies from 315 GHz to 410 GHz, 3, 6 and 10 dB below peak.

The peaks of the co- and cx-polar field values are given in Table 5-7

frequency	Co-polar	Cx-polar
GHz	dB	dB
315	68.60	32.12
334	68.52	30.74
353	68.43	30.25
382	68.14	34.49
410	67.82	37.61

Table 5-7 Co- and cx-polar peaks.

The averaged radiometer bandshape for the HFI_353_5b detector is found by a summation of the bandpass response values shown in Figure 5-19 in intervals from 19 GHz to 28 GHz around the center frequencies. The average levels are shown as blue lines in the figure.

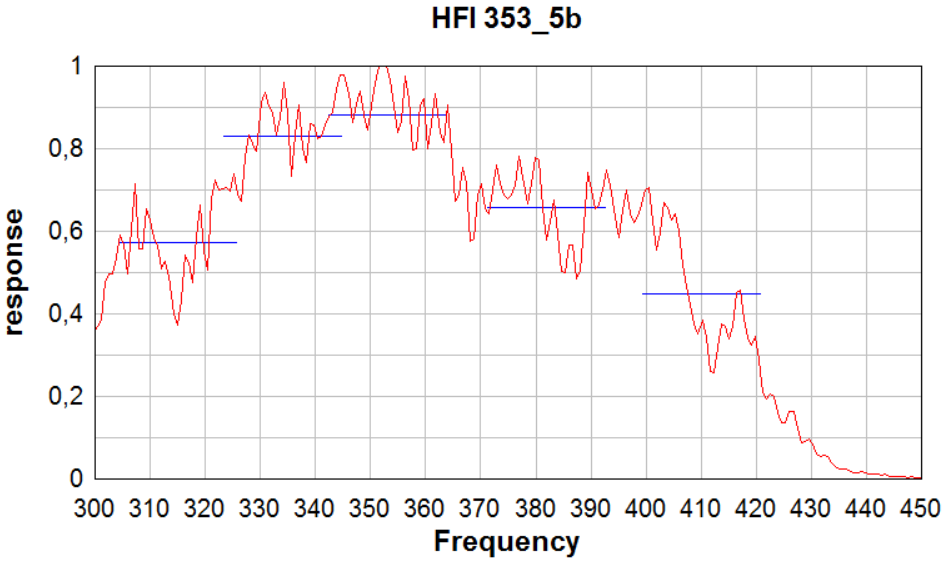

Figure 5-19 5 averaged bandpass responses for detector, HFI-353-5b.

The total bandpass pattern is found by multiplying these average response levels on the individual centre frequency beams and adding these in power, see Figure 5-20.

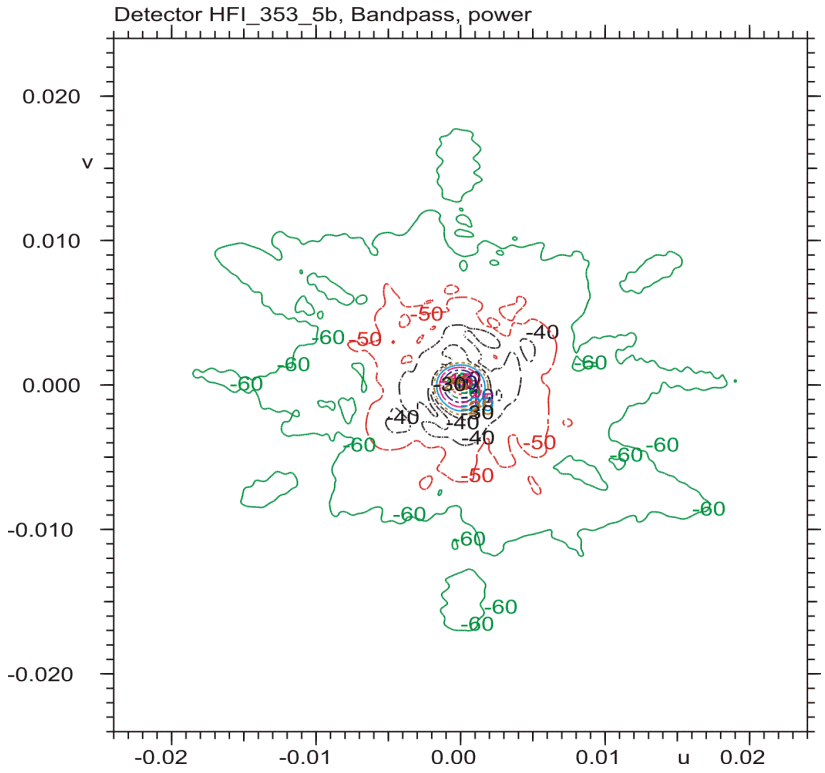

Figure 5-20 Bandpass main beam, detector HFI_353_5b.

In Figure 5-21 the bandpass pattern is shown together with the 353 GHz frequency pattern, which has been used for the HFI_353_5b detector in the previous retrievals. The two patterns are nearly identical.

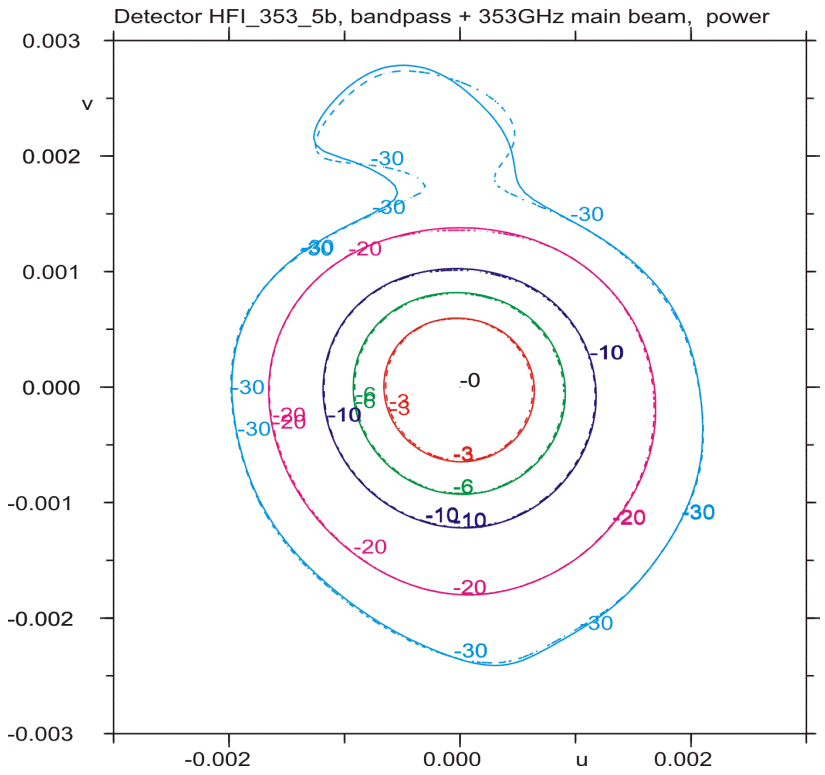

Figure 5-21 Bandpass (solid line) & 353 GHz beam (dashed).

The average pattern is compared with the single frequency beams at all the frequencies in Table 5-8, where the deviations are calculated down to different levels.

Rms[dB]	Frequency GHz				
Level	315	334	353	382	410
10 dB	0.31	0.17	0.05	0.23	0.46
20 dB	0.31	0.17	0.06	0.23	0.46

Table 5-8 Pattern deviations above level below peak.

The 353 GHz patterns is the best match to the average pattern for all levels below peak.

6. Conclusion.

The RF performances from the final retrieved telescope geometry, RFM2, are calculated for a selection of detectors at frequencies selected inside the frequency bands. RFM2 does not include mirror distortions from the quilting. It should also be noticed that no part of the Planck shields are used in the RF calculations.

The effect of the amplifier losses of the detectors at different frequencies in the frequency bands has also been evaluated by calculating the average power beams for the selected wide-band detectors.

References

Planck team (2007)
"Planck Parameter Definition Document"
PL-COM-IAS-SD-L2.02.005, dated 12-marts-2007.

K. Pontoppidan, 2005-2008
GRASP Technical Description

N. Chr. Albertsen, 2008
"Planck, RFFM Main beam computation", TICRA Report S-1496-3a, dated September 2008.

P. Nielsen, 2013
"In-flight Retrieval of Geometrical information on the Planck Telescope – RF performance of all detectors for first retrieved geometry, RFM1 ", S-1599-WP1, dated November 2013.

P. Nielsen, 2013
"In-flight Retrieval of Geometrical information on the Planck Telescope – RF performance in intermediate lobes for first retrieved geometry, RFM1 ", S-1599-WP2, dated November 2013.

P. Nielsen, 2015
"In-flight Retrieval of Geometrical information on the Planck Telescope – Geometry retrieval using combined HFI and LFI beam data", S-1563-13, dated December 2015.

P. Nielsen, 2015
"In-flight Retrieval of Geometrical information on the Planck Telescope RFM2 – RF performance of LFI beams", S-1563-14, dated December 2015.

P. Nielsen, 2015
"In-flight Retrieval of Geometrical information on the Planck Telescope RFM2 – RF performance of HFI beams", S-1563-15, dated December 2015.

A. Final RFM2 retrieved geometry

The final retrieved telescope geometry model, RFM2, is described by the following displacements and distortions defined in the telescope coordinate systems shown in Figure A-1.

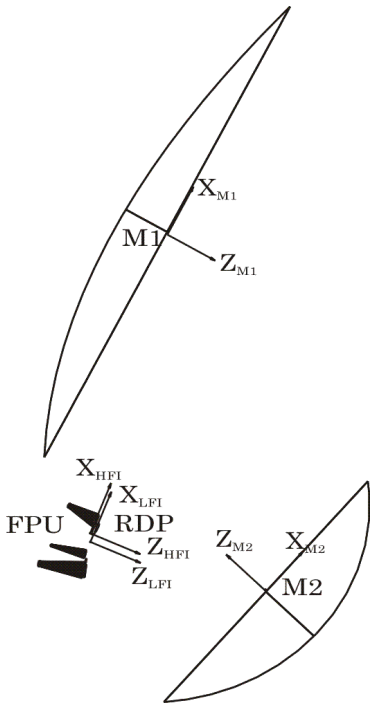

Figure A-1 Coordinate systems for RFM2.

The common LFI FPU coordinate system displacements are

- translation in X_{RDP}-direction of ÷0.06 mm
- translation in Y_{RDP}-direction of ÷0.01 mm
- translation in Z_{RDP}-direction of +0.05 mm
- rotation around the Z_{RDP}-axis of ÷4.1 arcmin

The common HFI FPU coordinate system displacements are

- translation in X_{RDP}-direction of +0.27 mm
- translation in Y_{RDP}-direction of ÷0.11 mm
- translation in Z_{RDP}-direction of +0.26 mm
- rotation around the Z_{RDP}-axis of +0.9 arcmin

All coordinate system displacements and rotations are relative to the respective NRFFM systems with the new detector positions described in Report S-1563-09.

The retrieved surface distortions on the reflectors are defined in the Z_{M1}- and Z_{M2}-directions and represented by the Zernike modes in Table A-1 and Table A-2.

Zernike mode		Amplitude	Rotation
m	n	[mm]	[degrees]
0	0	0.	0
0	2	-0.08	0
1	1	0.99	68
2	2	0.13	79
1	3	0.09	6
3	3	0.06	-58

Table A-1 Retrieved Zernike modes on main reflector.

Zernike mode		Amplitude	Rotation
m	n	[mm]	[degrees]
0	0	0.	0
0	2	0.00	0
1	1	1.37	-35
2	2	0.05	-69
1	3	0.29	-7
3	3	0.03	4

Table A-2 Retrieved Zernike modes on subreflector.

The LFI and HFI feed displacements in the individual retrieved FPU coordinate systems are given in Table A-3 and Table A-4, respectively.

Feed displacements	Deviation from retrieved RDP	
Detector	Δx [mm]	Δy [mm]
LFI18	0.03	0.11
LFI19	0.08	-0.13
LFI20	0.16	0.34
LFI21	-0.43	-0.36
LFI22	0.06	0.08
LFI23	0.15	0.00
LFI24	-0.20	-0.16
LFI25	-0.10	-0.05
LFI26	0.03	0.03
LFI27	-0.14	0.10
LFI28	-0.04	0.09

Table A-3 Retrieved LFI feed displacements.

Displacements	Deviation from RDP	
Detector	Δx [mm]	Δy [mm]
HFI-100-1	-0.05	0.00
HFI-100-2	-0.05	0.08
HFI-100-3	-0.02	0.09
HFI-100-4	**-0.12**	0.09
HFI-143-1	0.01	-0.01
HFI-143-2	0.02	-0.09
HFI-143-3	0.01	-0.08
HFI-143-4	0.01	-0.08
HFI-143-5	0.00	-0.05
HFI-143-6	-0.02	-0.11
HFI-143-7	-0.04	**-0.12**
HFI-217-1	0.04	0.04
HFI-217-2	0.05	0.09
HFI-217-3	0.05	0.14
HFI-217-4	-0.04	0.23
HFI-217-5	0.08	0.07
HFI-217-6	0.03	0.00
HFI-217-7	0.00	0.11
HFI-217-8	0.06	**0.11**
HFI-353-1	0.09	0.02
HFI-353-2	0.07	-0.07
HFI-353-3	0.09	0.03
HFI-353-4	0.10	0.01
HFI-353-5	**0.11**	0.06
HFI-353-6	0.09	0.05
HFI-353-7	0.06	0.01
HFI-353-8	-0.03	-0.01
Average	0.02	0.02

Table A-4 Retrieved HFI feed displacements.

B. Residue Function

The residual function for comparing patterns is defined as

$$f_i = w_i(p_{1,i} - p_{2,i} - \mu) = w_i(\Delta_i - \mu)$$

With the following parameters

i the subscript referring to the signal direction

w_i the weight factor given at the square root of the power and normalized to 1 at maximum.

$p_{1,i}$ the first signal power given in dB in direction i

$p_{2,i}$ the second signal power given in dB in direction i

Δ_i the power difference: $\Delta_i = p_{1,i} - p_{2,i}$

μ the weighted mean value:

$$\mu = \sum_{i=1}^{N} {w_i}^2 \Delta_i \; / \sum_{i=1}^{N} {w_i}^2$$

The squared variance to be minimized is then

$$\delta^2 = \sum_{i=1}^{N} {f_i}^2 \; / \sum_{i=1}^{N} {w_i}^2$$

Only directions where the field is above a specific level are used in the summation.